NASA Technical Memorandum 4171

Experimental Characterization of the Effects of Pneumatic Tubing on Unsteady Pressure Measurements

Stephen A. Whitmore
Ames Research Center
Dryden Flight Research Facility
Edwards, California

William T. Lindsey
Air Force Wright Aeronautical Laboratory
Wright-Patterson Air Force Base, Ohio

Robert E. Curry and Glenn B. Gilyard
Ames Research Center
Dryden Flight Research Facility
Edwards, California

National Aeronautics and
Space Administration
Office of Management
Scientific and Technical
Information Division

1990

CONTENTS

SUMMARY

Advances in aircraft control system designs have, with increasing frequency, required that airdata be used as flight control feedbacks. This requirement makes it essential for these data to be measured with accuracy and high fidelity. Most airdata information is provided by pneumatic pressure measuring sensors. Typically unsteady pressure data provided by pneumatic sensing systems is distorted at high frequencies. The distortion is a result of the pressure being transmitted to the pressure sensor through a length of connective tubing. The pressure is distorted by frictional damping and wave reflection. As a result, airdata provided by all-flush, pneumatically sensed airdata systems may not meet the frequency response requirements necessary for flight control augmentation.

To investigate the effects of this high-frequency distortion in remotely located pressure measurement systems, both lab and flight tests were performed at the NASA Ames Research Center's Dryden Flight Research Facility. Good qualitative agreement between the lab and flight data are demonstrated. Results from these tests are used to describe the effects of pneumatic distortion in terms of a simple parametric model.

INTRODUCTION

Recent advances in aircraft performance and maneuverability have dramatically complicated the problem of flight control augmentation. With increasing frequency, control system designs require that aerodynamic parameters such as angle of attack and dynamic pressure be used as feedbacks. This design philosophy requires that these data be measured with accuracy and high fidelity. Typically these frequency response requirements are approximately 20 Hz. Most airdata information is provided by pneumatic pressure sensing systems. Unsteady pressure measurements may be distorted at high frequencies because the pneumatic pressure sensing systems transmit pressure through a length of connective tubing. Primarily, pressure distortion results from frictional damping along the tubing walls. Cavity resonance results from the reflection of pressure waves at the transducer end back up the tubing.

A research effort was initiated at the NASA Ames Research Center's Dryden Flight Research Facility to investigate the effects of this high frequency distortion in pressure measurement systems. These tests were sponsored in part by the Air Force Wright Aeronautical Laboratory. Both lab and flight tests were performed. The procedures and equipment used to obtain the data are presented. The resulting laboratory and flight data are presented. The lab and flight tests were used to describe the effects of pneumatic distortion within the pressure tubing in terms of a simple parametric model. Lab and flight results are compared using this parametric model.

NOMENCLATURE

c	sonic velocity
D	pressure tubing cross-sectional diameter
ESP	electronically scanned pressure
L	length of pneumatic tubing
M	Mach number

M_r	magnitude ratio of first resonant peak
M_B	magnitude ratio at 40 dB/decade rolloff frequency
PCM	pulse code modulation
P_I	sensor input pressure
P_M	measured sensor pressure
$U(x,t)$	average wave speed at location x
x	longitudinal spatial coordinate
ξ	damping ratio of second-order model
ρ	density
τ_L	time lag of second-order model
ω_B	frequency at which magnitude rolls off at 40 dB/decade
ω_n	natural frequency of second-order model
ω_r	frequency of first resonant peak

GENERAL CONSIDERATIONS

The typical pneumatic sensing system to be considered may be modeled as a straight cylindrical tube with an axisymmetric volume attached at its downstream end. The tube represents the transmission line from the surface to the sensor (fig. 1). The tube is considered to be of constant diameter, D, with length, L. Since most modern high fidelity pressure transducers have a negligible internal volume, it is assumed that the frequency response capability of the pressure transducer is far greater than that of the pneumatic tubing. This study attempts only to characterize the distortion induced by the pneumatic tubing.

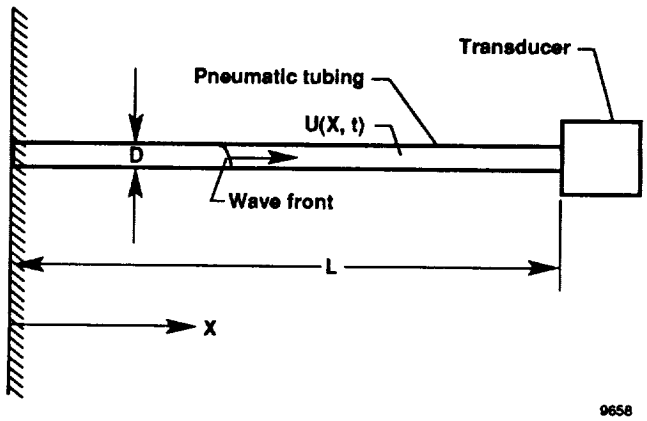

Figure 1. Pneumatic pressure sensing system.

LABORATORY TESTS: EQUIPMENT, PROCEDURES, AND RESULTS

Laboratory tests were performed to determine the frequency response characteristics of various tubing geometries. Figure 2 shows the arrangement of the instruments used to perform the tests. The equipment consisted of:

1. An acoustical amplifier with adjustable volume and frequency output; the amplifier is capable of outputting a pure tone, adjustable from 0 to 2000 Hz. The amplifier cylinder cavity was fitted with a pressure fixture which allowed the internal pressure to be either elevated or lowered to simulate the effects of altitude,
2. an absolute pressure transducer, range 0.0–50.0 lb/in^2 absolute, with ±0.5-percent accuracy,
3. steel tubing sections, with lengths ranging from 0.35 to 10.89 ft and interior diameters ranging from 0.021 to 0.125 in.,
4. a miniature strain gage differential pressure transducer; range ± 2.0 lb/in^2 differential, with ±2.50-percent accuracy mounted in the head of the acoustical amplifier,
5. the test transducer; a high frequency, 32-port, silicon-diaphragm, piezoresistive, differential, electronically scanned pressure (ESP) module; range ±5.0 lb/in^2 differential, with ±2.50-percent accuracy, having a very small internal volume (0.001 in^3); the ESP module is depicted in figure 3,
6. an analog spectral analyzer which accepts two inputs, transforms them into relative magnitude and phase, and displays the resulting spectra on a logarithmic plotting device,
7. two oscilloscopes to display the time responses of the test and reference sensors, and
8. a plotting device to record the spectral plots.

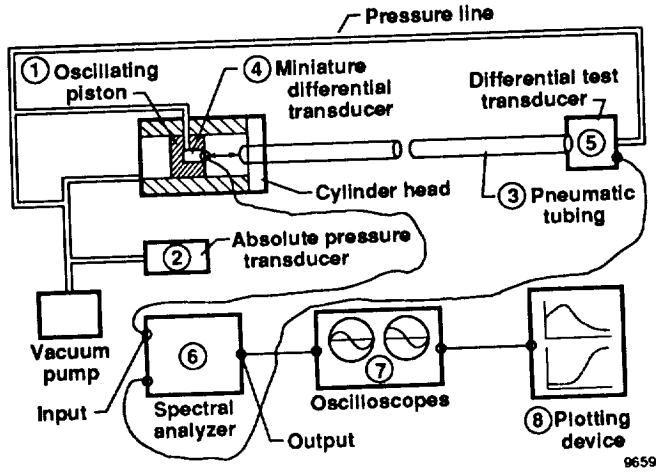

Figure 2. Laboratory setup for frequency response tests.

The test procedure consisted of comparing the frequency response of a transducer, mounted at the end of a section of connective tubing, relative to that of a known pressure input. A single input port of the ESP module was attached to the downstream end of the tubing test section; this port served as the test sensor. The strain-gage transducer was mounted in the head of the amplifier to enclose zero internal volume; this transducer served as the test sensor.

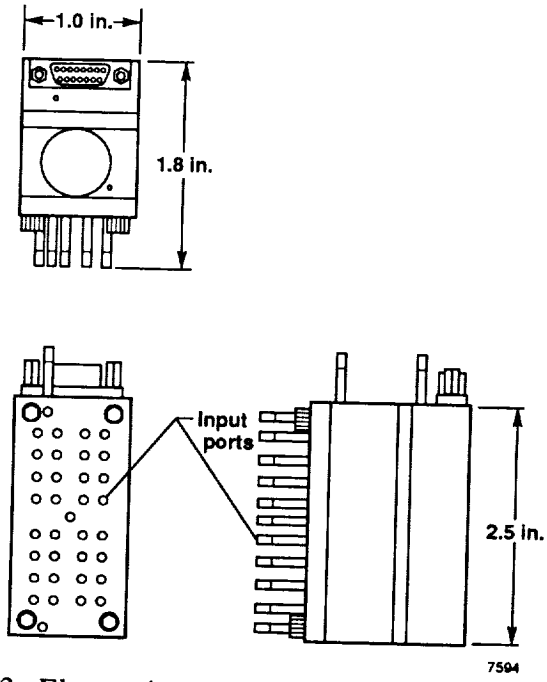

Figure 3. Electronic scanning pressure (ESP) transducer.

The ESP module was vented to room pressure at the backside. The reference transducer, also a differential sensor, was vented to the system cavity on the backside. Differences between absolute pressure within the system cavity and room pressure were accounted for by adjusting the gains on the output signals.

The pressure within the amplifier cylinder cavity was lowered to simulate a desired altitude and a frequency sweep was performed. All lab tests were performed at room temperature (approximately 70 °F). The responses of the test and reference sensors were passed through the spectral analyzer, converted to relative magnitude, and expressed in polar form. The resulting magnitude and phase were plotted as a function of frequency. The tests were repeated for several of the test sections at a variety of base pressures (altitudes).

Figures 4 and 5 present Bode plots in which both magnitude and phase angle are shown (ref. 7). Figure 4 depicts the frequency response of a test configuration with 48.5 in. of 0.021-in. steel tubing obtained with the system at ambient pressure (2300-ft altitude). Figure 5 shows the frequency response of a test configuration with 48.5 in. of 0.06-in. steel tubing at 2300-ft altitude. The first case is over damped since the response rolls off quickly beyond 10 Hz. On the other hand, the second case is under damped since it exhibits a resonant peak of approximately 50 Hz.

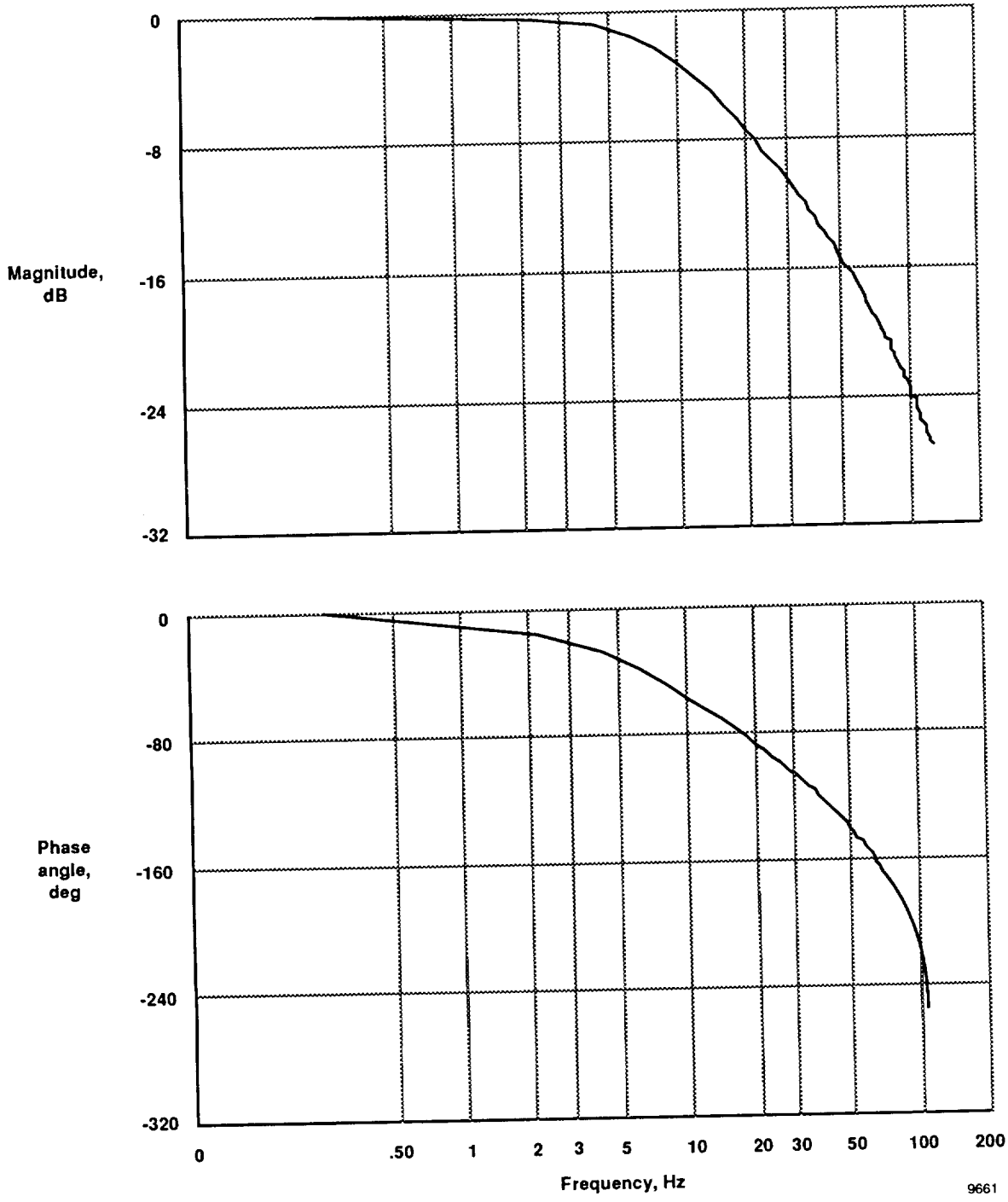

Figure 4. Lab frequency response data: tubing L = 48.5 in., D = 0.02 in., altitude = 2300 ft.

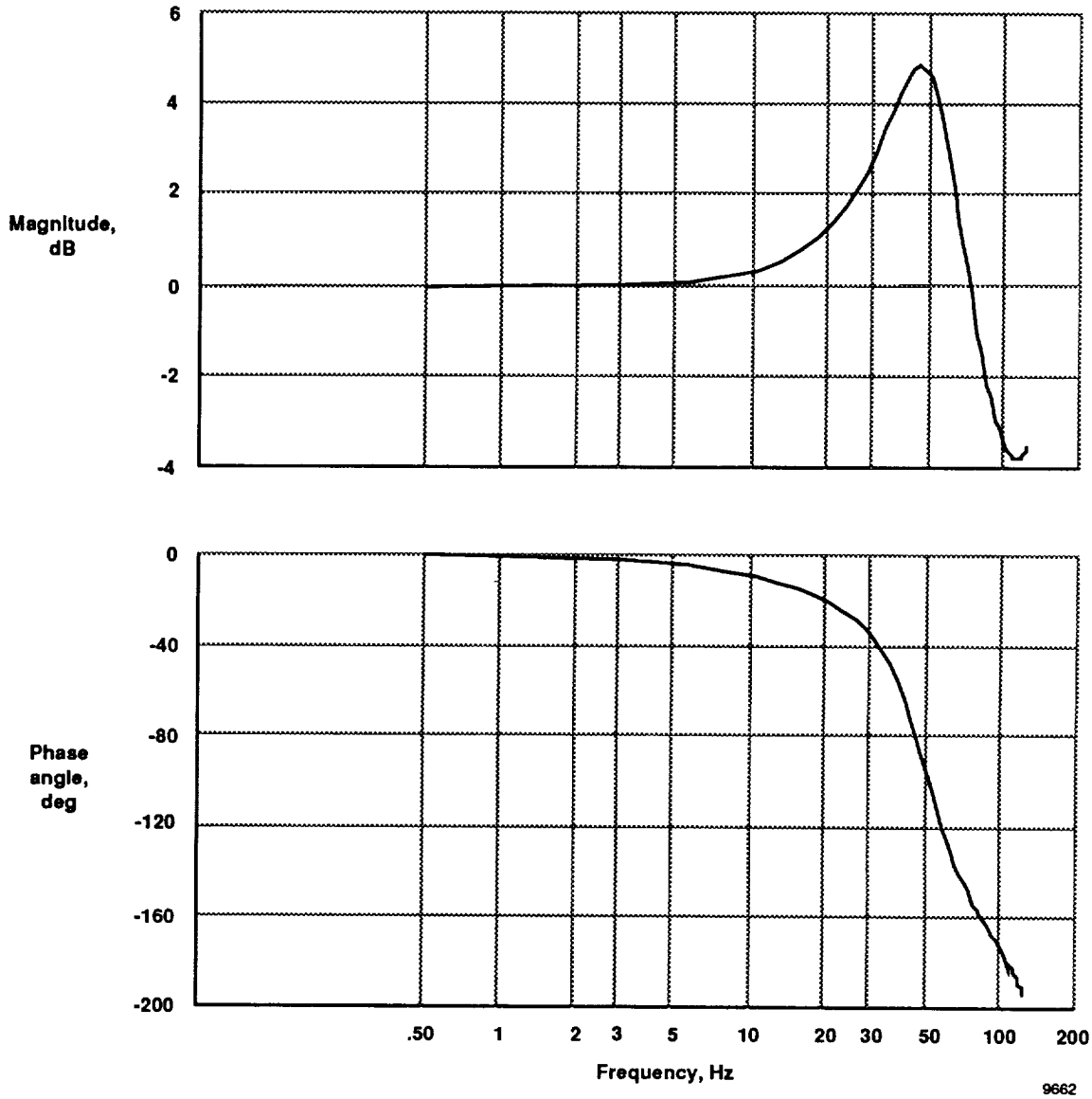

Figure 5. Lab frequency response data: tubing L = 48.5 in., D = 0.06 in., altitude = 2300 ft.

FLIGHT TEST EQUIPMENT, PROCEDURES, AND RESULTS

The flight experiment design considerations were similar to that of the laboratory experiments. The hardware for this experiment was installed in the right-hand wing of an F-15 research aircraft. An access panel on the leading edge was used to install various test orifices and system hardware.

The flight-test configuration, figure 6, consisted of a set of static test orifices with diameters of 0.02, 0.04, and 0.06 in. Data were obtained from two groups of pressure orifices. Group 1 was situated at the 10-percent chord, 40-percent span, group 2 was located approximately 12 in. outboard. Reference measurements were provided by a thin, very low volume, high-frequency piezoelectric wafer pressure transducer, glued to the aircraft skin adjacent to group 1.

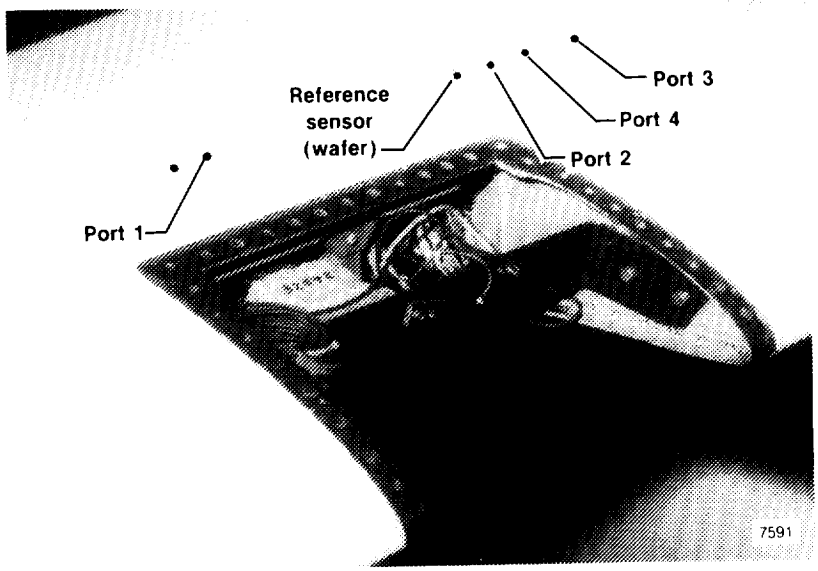

Figure 6. Flight test configuration.

The pressure ports of the test matrix were designed to allow for tubing sections to be interchangeable so that various tubing geometries could be evaluated. Individual test ports were fabricated using short pieces of metal tubing (approximately 1 in.) with internal diameters of 0.02, 0.04, and 0.06 in. A washer was soldered around the tubing 0.25 in. from one end. The entire piece was inserted into the aircraft skin from inside the wing through holes of corresponding diameters. The washer was cemented in place from the inside. The short external stem of tubing was filed flush with the surface of the wing. Flexible tubing of various lengths was run from the orifices to an ESP module identical to that used in the lab tests. A schematic of the flight-test configuration is depicted in figure 7. Test ports 1 and 2 had tubing diameters of 0.06 in., test port 3 a tubing diameter of 0.04 in., and test port 4 a tubing diameter of 0.02 in. The test ports, port diameters, and tubing lengths and diameters used during the flight tests are tabulated in table 1.

Table 1. Test port diameters, tubing lengths, and diameters used for flight test experiment.

Port number	Diameter	Transducer type	Volume, in^3	Tubing diameter, in.	Tubing length, ft
Ref.	---	Surface mounted wafer	0.000	---	---
1	0.06	ESP	0.001	0.06	0.5
2	0.06	ESP	0.001	0.06	2.0, 4.0, 8.0
3	0.04	ESP	0.001	0.04	2.0, 4.0, 8.0
4	0.02	ESP	0.001	0.02	2.0, 4.0, 8.0

The diameter of each ESP input port is 0.04 in. Each port is connected to 0.59 in. of external metal tubing. The flexible tubing sections of various lengths and diameters were slipped over this external tubing. The ESP module multiplexed the individual port measurements and the resulting signal was sent to a 10-bit pulse code modulation (PCM) system, sampled, time-tagged, and recorded on onboard tape at a rate of 500 samples/sec. The ESP module transducers were ranged for ± 5.00 lb/ft^2-differential. The ESP module environment was controlled by wrapping the transducer in a heater blanket to eliminate temperature shifts.

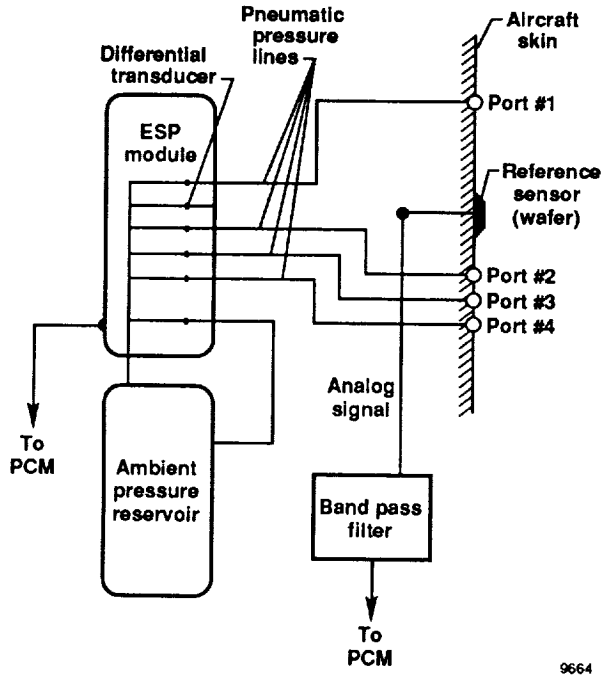

Figure 7. Flight test configuration.

As mentioned earlier, since the ESP module is a differential pressure sensor, backside reference pressure was provided by a damping reservoir which contains a large internal volume. This reservoir was stored in the wing cavity, and the pressure within this reservoir was sensed by a 0–15 lb/in^2 absolute pressure transducer. The estimated uncertainty in the sampled output from the ESP module is ± 2.50 percent of full scale. The output resolution was approximately 0.25 lb/ft^2. Reference pressure measurements were provided by a piezoelectric wafer pressure transducer glued to the aircraft skin. Since the reference transducer was mounted external to the aircraft skin, its environment could not be controlled. Specifically, the temperatures experienced by the transducer were considerably lower than those recommended for the normal operating range of the transducer. This caused the steady-state output to eventually drift off scale. To eliminate this drift, the reference sensor output was electronically coupled with a passive second-order, band-pass filter to remove the steady-state component. This also eliminated any aliasing problems. The filter pass band extended from 1.16 to 101.7 Hz. The analog output from the reference transducer–bandpass filter was passed to the aircraft PCM system, sampled at 500 samples/sec, time tagged, and recorded on onboard tape. The estimated uncertainty in the sampled output is ± 2.0 percent of full scale. The output resolution is 0.25 lbf/ft^2.

The following procedure was used to obtain the flight data which was used to perform frequency response analyses. With the aircraft engine set at a constant power setting, the pilot rolled into a 2.5-g windup turn at constant Mach number (M) and altitude. During these maneuvers, high angles of attack would be reached. This induced a leading-edge flow which caused unsteady, broad-band pressure variations at the sensor matrix.

Two representative time history cases are presented in figures 8 and 13. The corresponding frequency response data are shown in figures 9 through 12, and figures 14 through 17, respectively.

Figure 8 illustrates time history data obtained at an altitude of 22,800 ft and Mach 0.65. Presented from bottom to top respectively, are the pressure readings obtained from the wafer reference sensor, port 1 with 0.5 ft of 0.06-in. diameter tubing; port 2 with 8.0 ft of 0.06-in. diameter tubing; port 3 with 8.0 ft of 0.04 -in. diameter tubing; and port 4 with 8.0 ft of 0.02-in. diameter tubing.

The corresponding frequency response data are presented in figures 9 through 12. The individual frequency responses of ports 1 through 4 are shown relative to the reference sensor. Test sensor 1 shows a sizable resonance in the neighborhood of 200 Hz. Test sensors 2, 3, and 4 all show gradually higher damping as the tubing diameter is decreased. The phase lag of the output signals gradually increases

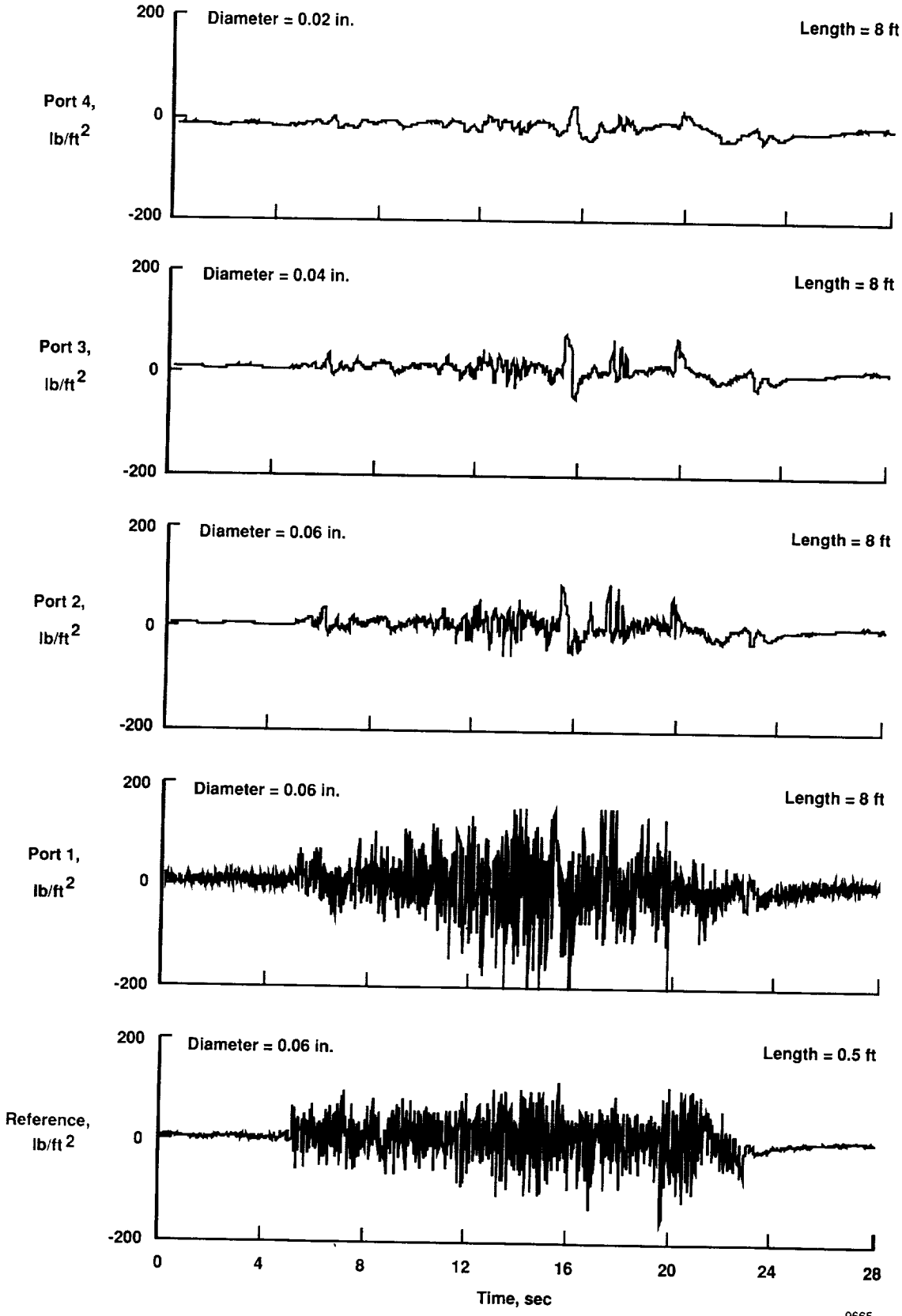

Figure 8. Flight-test configuration pressure data at 22,800 ft altitude and $M = 0.65$.

as the tubing damping grows larger. These results are as expected and are qualitatively consistent with the lab results.

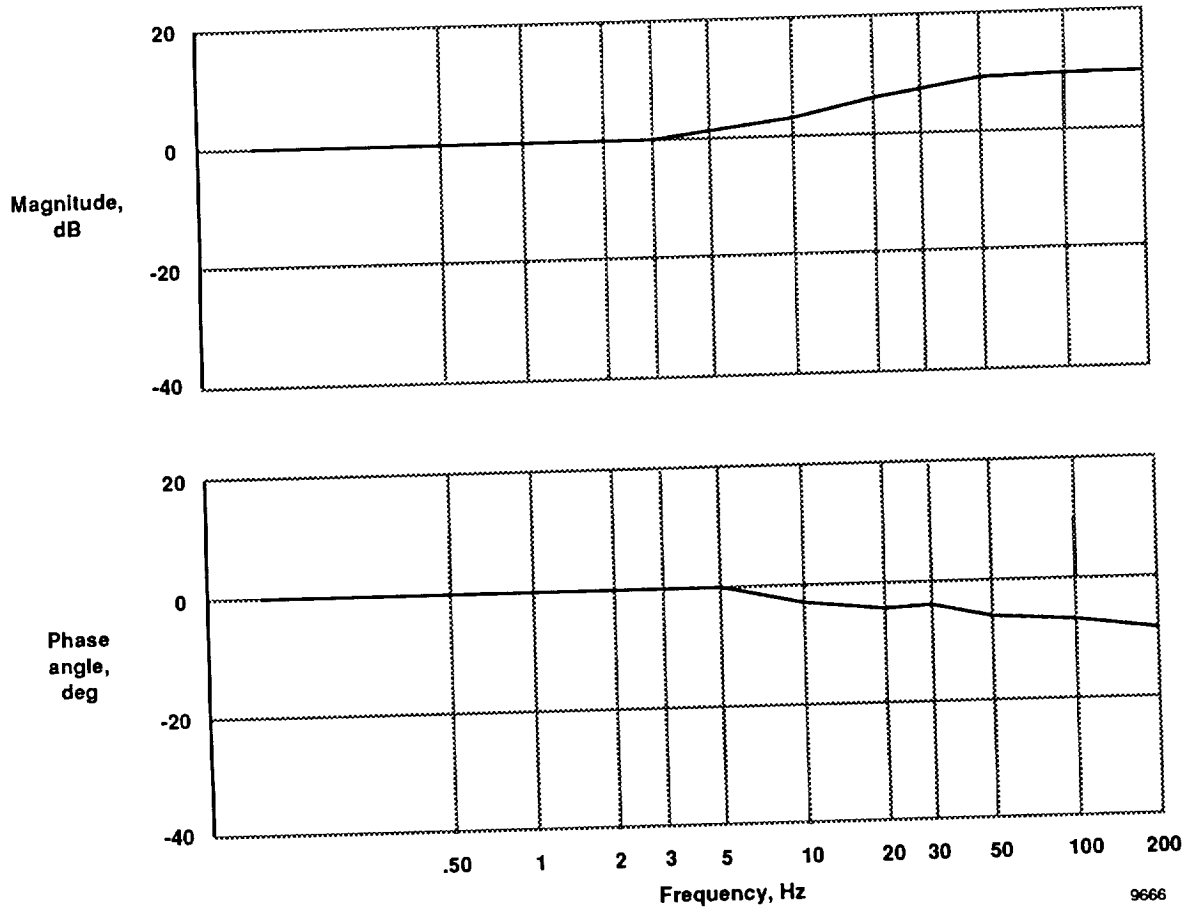

Figure 9. Frequency response for port 1 with 0.5 ft of 0.06-in. diameter line.

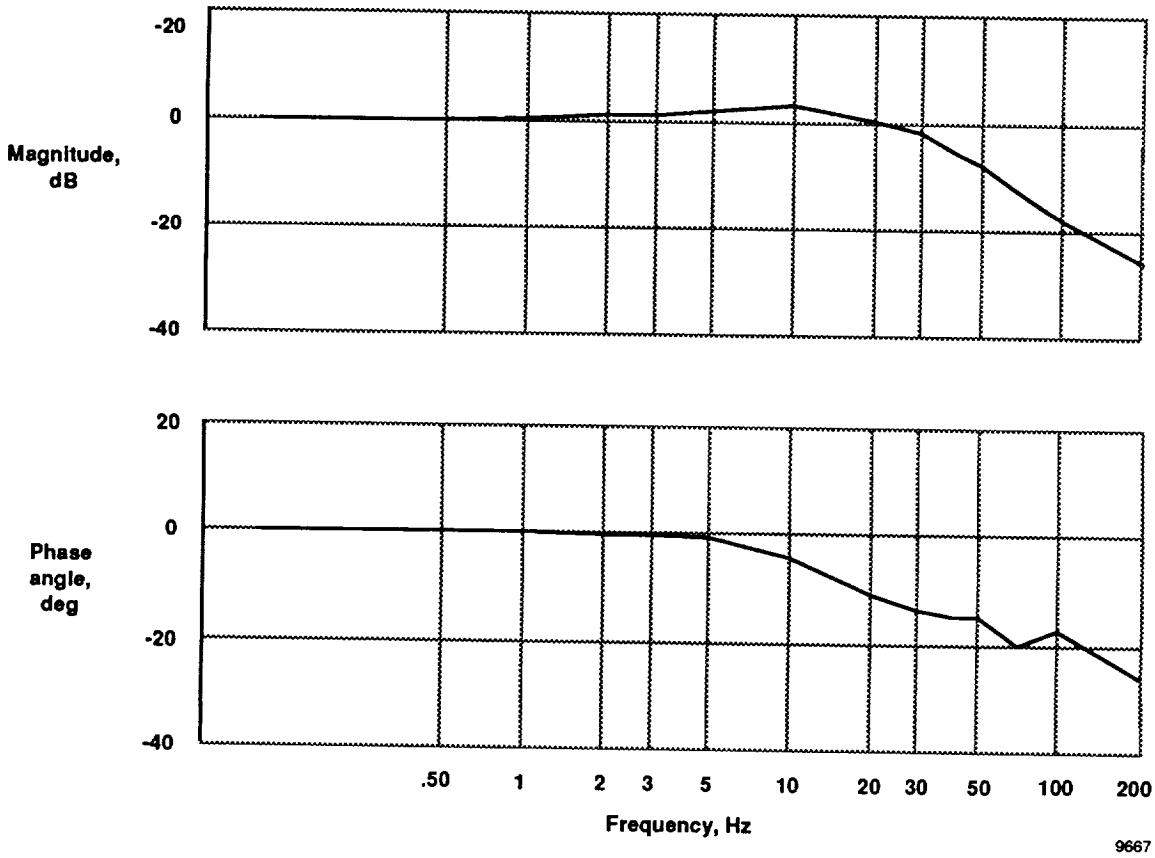

Figure 10. Frequency response for port 2 with 8.0 ft of 0.06-in. diameter line.

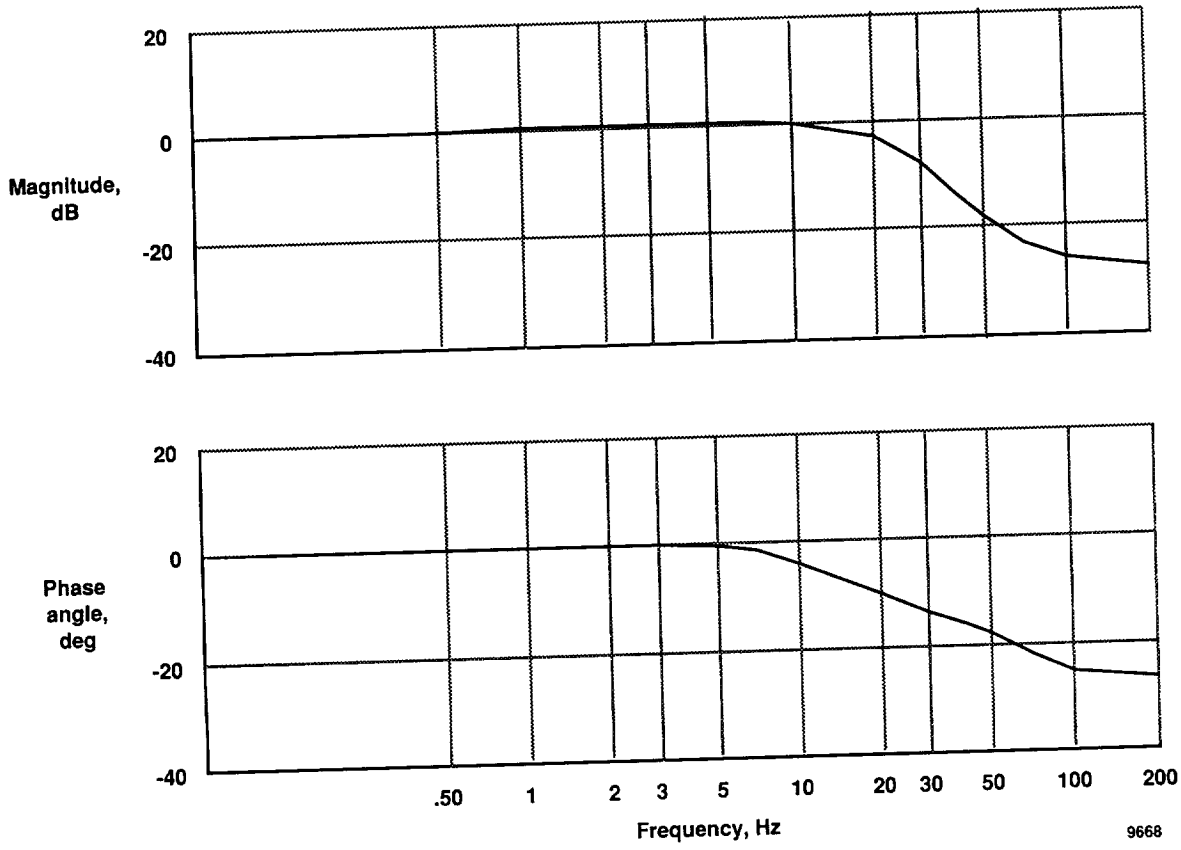

Figure 11. Frequency response for port 3 with 8.0 ft of 0.04-in. diameter line.

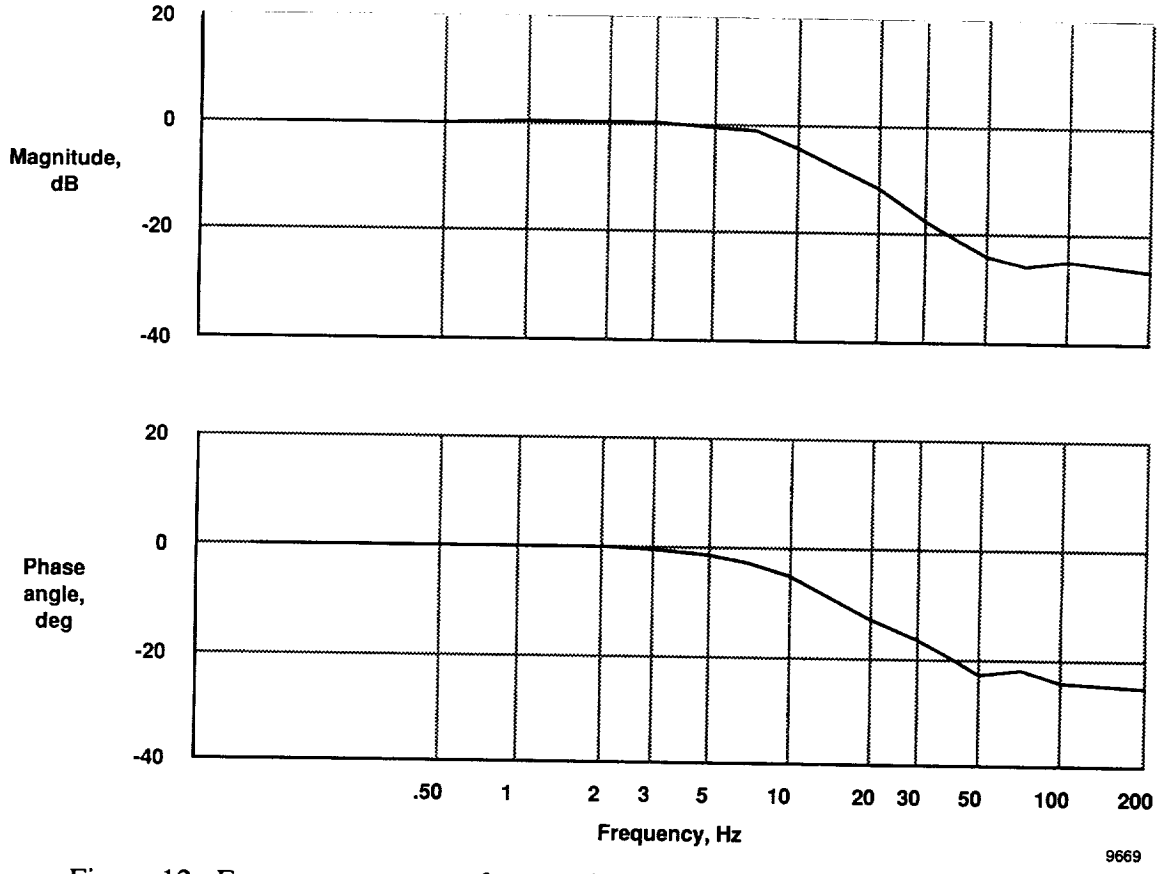

Figure 12. Frequency response for port 4 with 8.0 ft of 0.02-in. diameter line.

Presented in figure 13 are time history data obtained at an altitude of 19,800 ft and Mach 0.62. Presented, from bottom to top respectively, are the pressure readings obtained from the wafer reference sensor, the port 1 with 0.5 ft of 0.06-in. diameter tubing; port 2 with 2.0 ft of 0.06-in. diameter tubing; port 3 with 2.0 ft of 0.04-in. diameter tubing; and port 4 with 2.0 ft of 0.02-in. diameter tubing.

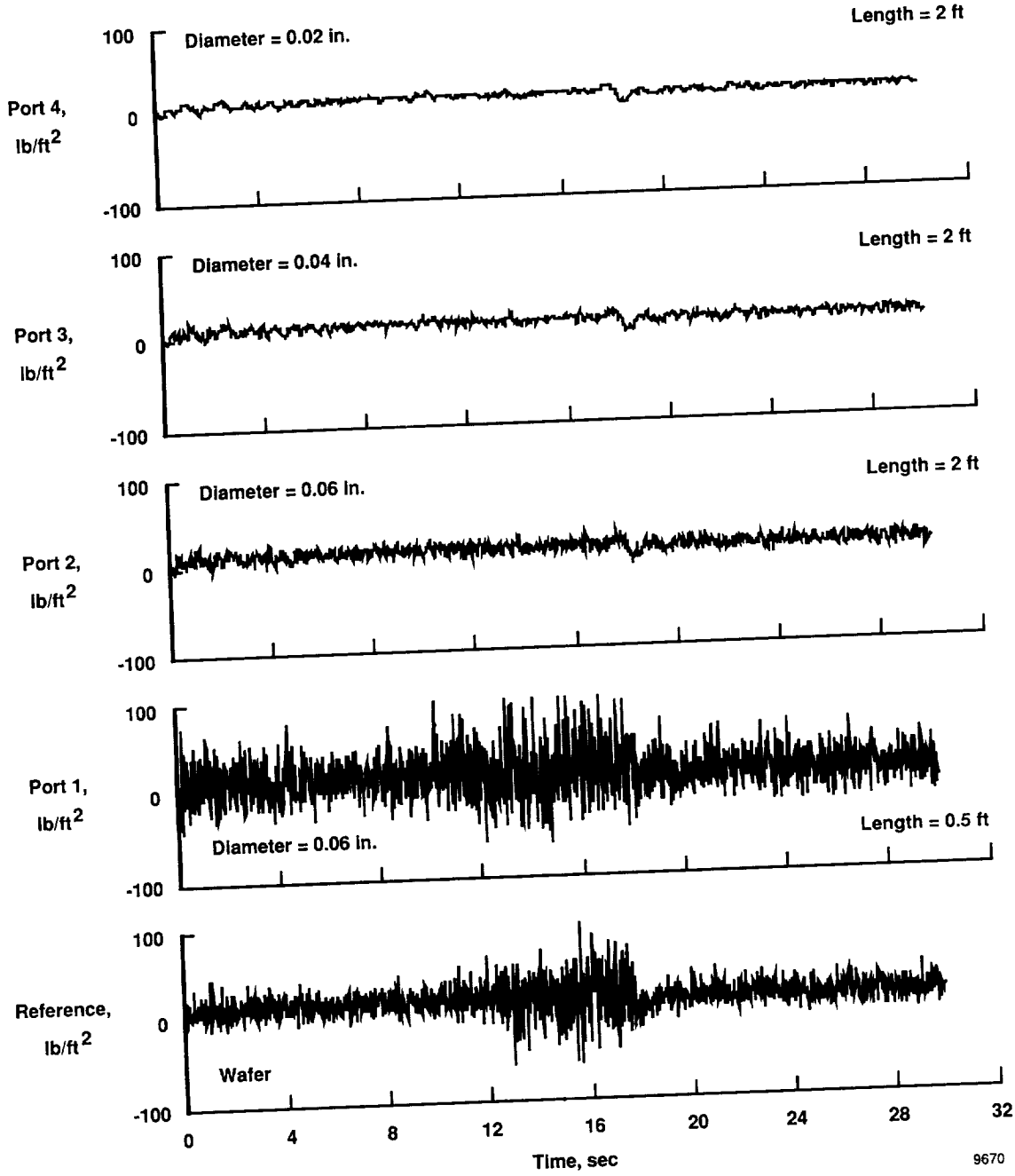

Figure 13. Flight-test configuration pressure data at 19,800 ft altitude and $M = 0.62$.

The corresponding frequency response data are depicted in figures 14 through 17. As previously noted, the individual frequency responses of ports 1 through 4 relative to the reference sensor are presented. Note that the port 1 output shows resonant behavior similar to the output in figure 9; whereas the outputs from the ports with the 2.0-ft line lengths show less damping than in figures 10 through 12.

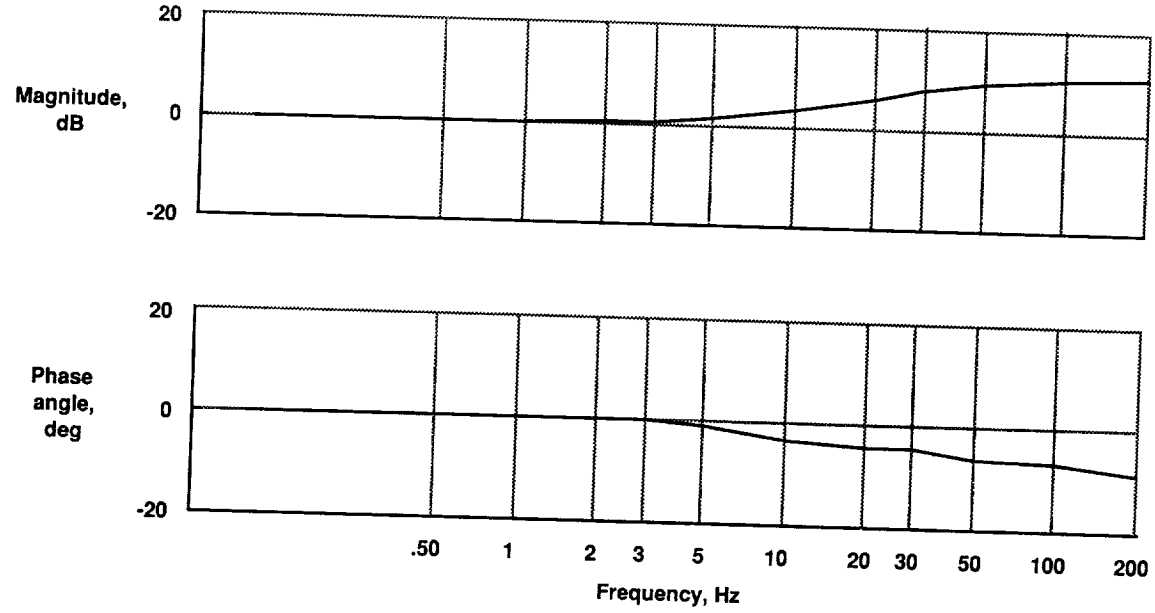

Figure 14. Frequency response for port 1 with 0.5 ft of 0.06-in. diameter line.

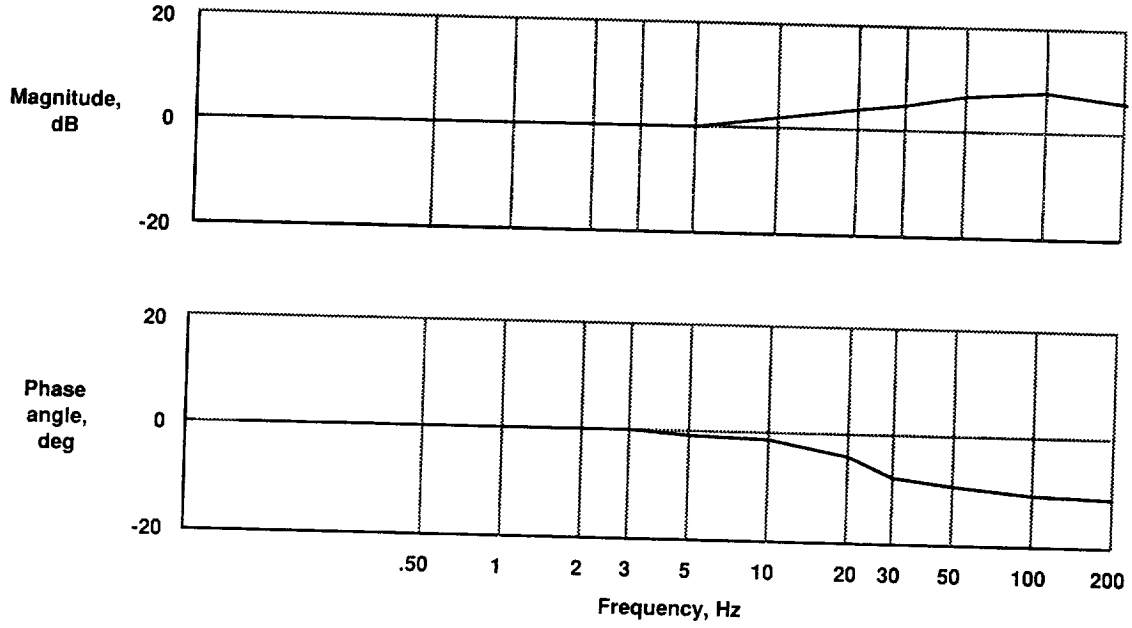

Figure 15. Frequency response for port 2 with 2.0 ft of 0.06-in. diameter line.

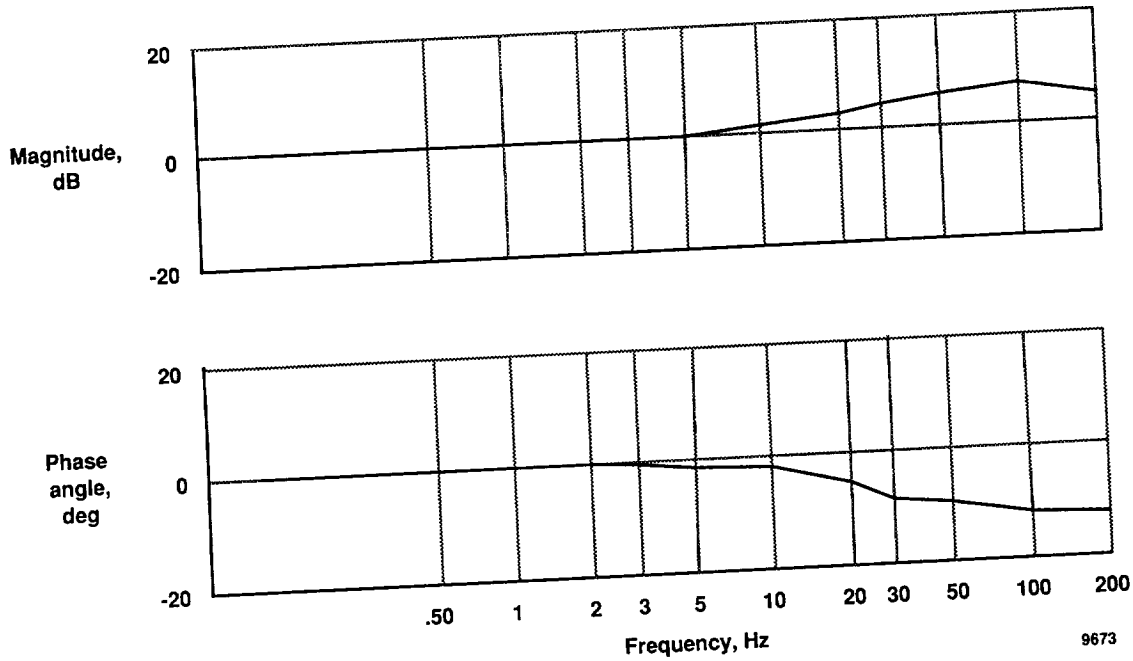

Figure 16. Frequency response for port 3 with 2.0 ft of 0.04-in. diameter line.

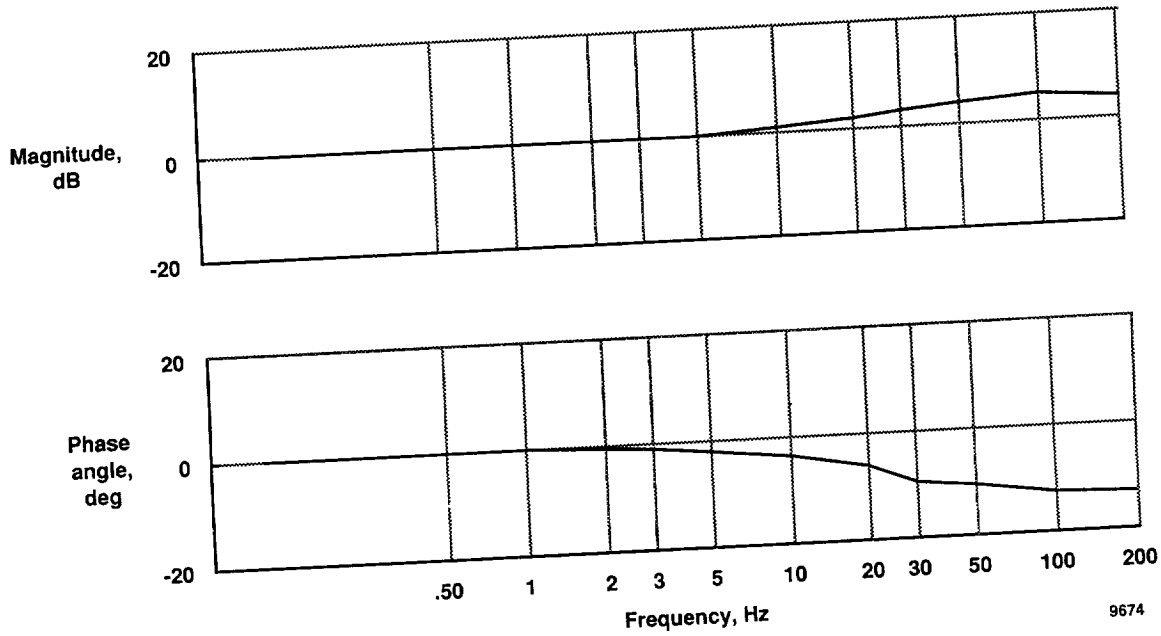

Figure 17. Frequency response for port 4 with 2.0 ft of 0.02-in. diameter line.

PARAMETRIC MODEL

Using the second-order dynamics model in the appendix, the results of both the lab and flight tests are summarized in the following order: lab results, flight results, and a comparison of the results.

Parametric Summary of Lab Data

Parametric curves which describe ξ and ω_n for the lab data as a function of the pressure tubing geometry and altitude are presented in figures 18 through 21. Figure 18 shows the sensor damping ratio plotted against tubing length for a variety of tubing diameters. As the tubing length approaches zero, the damping ratio of the system approaches zero. The damping ratio decreases as the diameter of the tubing is increased.

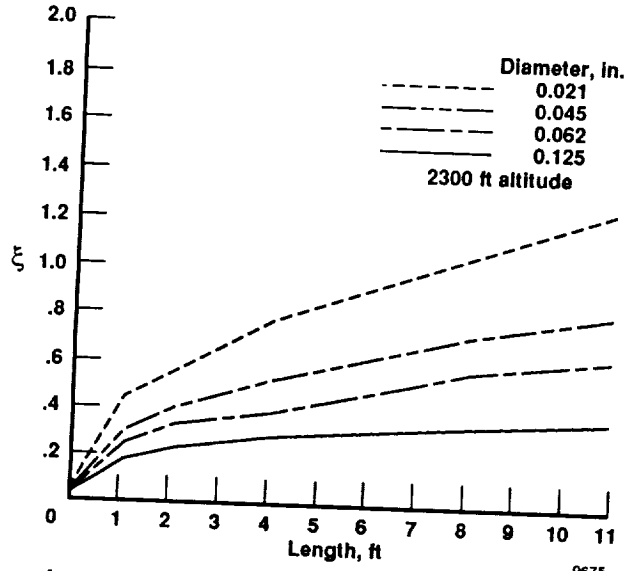

Figure 18. Lab results: damping ratio as a function of pressure tubing geometry.

Figure 19 presents the sensor natural frequency plotted against tubing length for a variety of tubing diameters. As the tubing length approaches zero, the natural frequency of the system grows rapidly. There is only a slight effect on the natural frequency as the diameter of the tubing is changed. The sensor is behaving like a tuned pipe where the natural vibration frequency is primarily a function of length only (ref. 8).

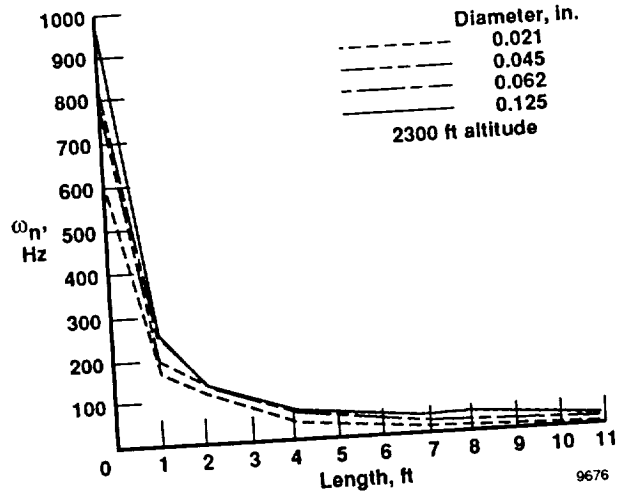

Figure 19. Lab results: natural frequency as a function of pressure tubing geometry.

Parametric curves are presented in figures 20 and 21 which describe ξ and ω_n as a function of the altitude for several different tubing geometries. Figure 20 shows the sensor damping ratio plotted against altitude for a variety of tubing geometries. In all cases, the damping ratio increases proportionately with altitude. As altitude increases air density decreases and the wave is not as easily sustained, thus, the sensing system will appear to be more highly damped. Figure 21 presents the sensor natural frequency plotted against altitude for a variety of tubing geometries. In all cases the natural frequency remains constant with increasing altitude. References 2 and 8 have demonstrated that the natural frequency of the sensor is primarily a function of local sonic velocity and tubing length. The local sonic velocity remained constant because the lab experiments did not simulate temperature effects at altitude.

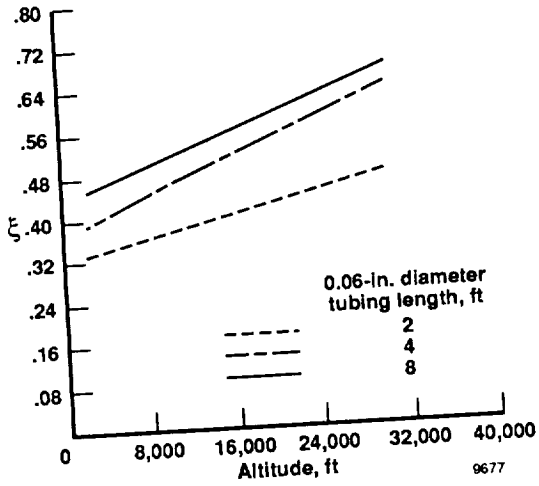

Figure 20. Lab results: damping ratio as a function of altitude.

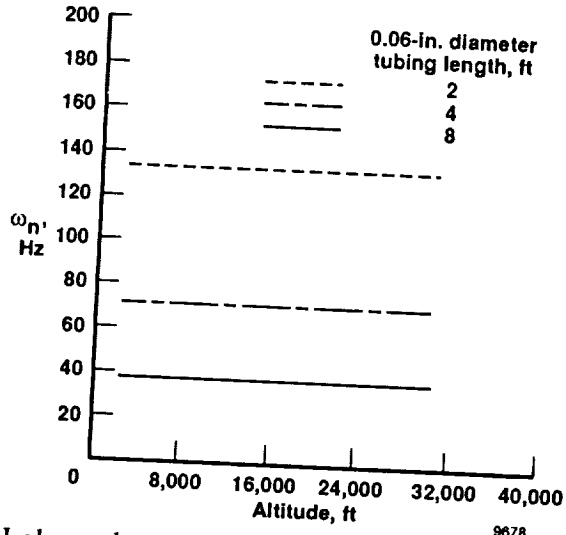

Figure 21. Lab results: natural frequency as a function of altitude.

Parametric Summary of Flight Data

Results of the flight tests are summarized by plotting values for ξ and ω_n as a function of the pressure tubing geometry and pressure altitude. These data are plotted as a function of tubing geometry in figures 22 and 23. The parameters are plotted as a function of the altitude for several different tubing geometries in figures 24 and 25. In figure 25, the natural frequency shows a slight drop as a function of altitude.

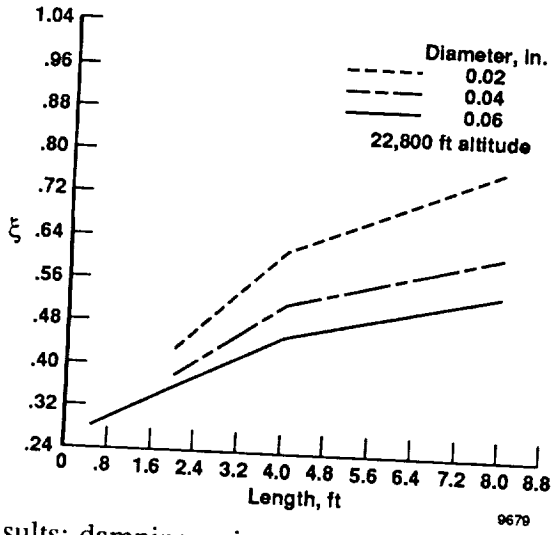

Figure 22. Flight results: damping ratio as a function of pressure tubing geometry.

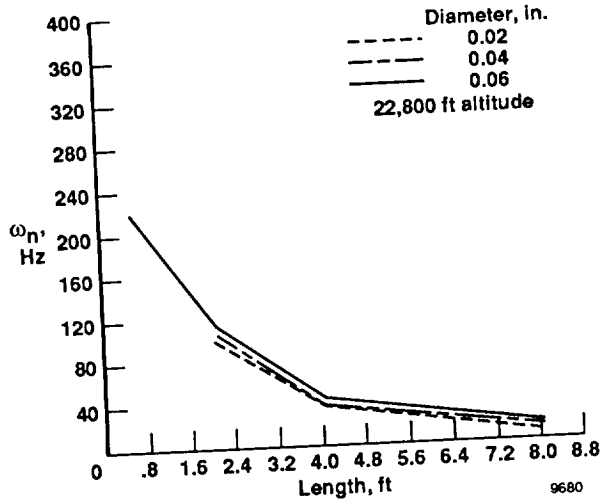

Figure 23. Flight results: natural frequency as a function of pressure tubing geometry.

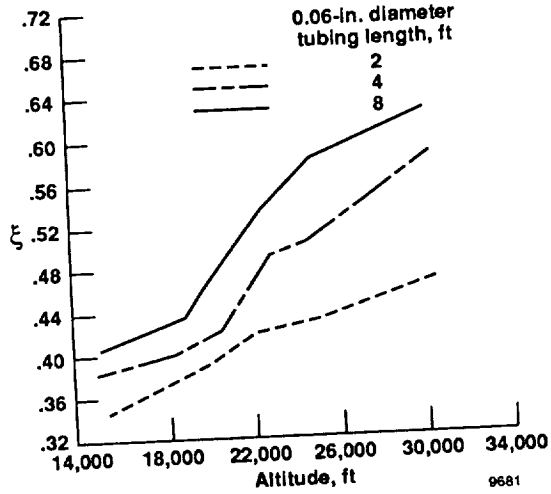

Figure 24. Flight results: damping ratio as a function of altitude.

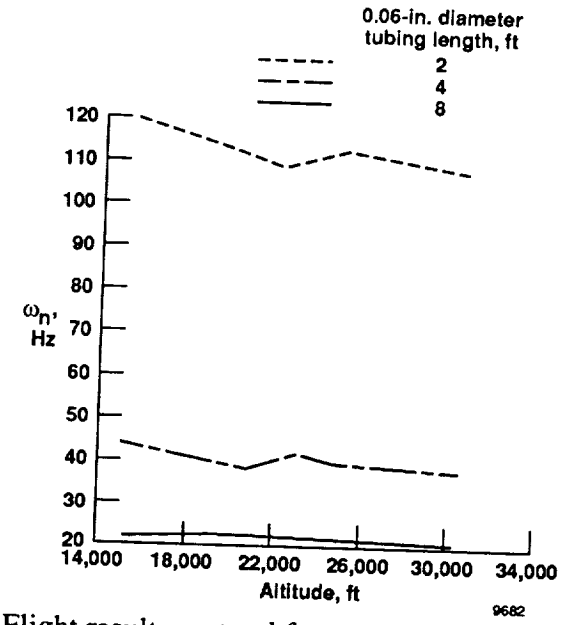

Figure 25. Flight results: natural frequency as a function of altitude.

Comparison of Flight and Lab Test Results

For comparison purposes, lab data taken from figures 20 and 21 are superimposed upon the flight in figures 26 and 27. In these figures, ξ and ω_n are plotted as a function of altitude for 0.06-in. diameter tubing with lengths of 2.0, 4.0, and 8.0 ft, respectively. The lab and flight results, while being qualitatively similar, do not agree quantitatively. In general, the lab data indicate both a higher damping ratio and higher natural frequency than do the flight data. As mentioned earlier, natural frequencies obtained from the flight data show a slight drop as altitude increases; the lab data do not. The disagreements between the lab data and the flight data are most likely a result of the lab data being obtained at higher temperatures than were the flight data. The lab tests were performed at 70 °F; whereas the flight data were obtained at ambient temperatures ranging from -15 to 10 °F. Thus for a given test pressure altitude, the flight data were obtained at a higher density, higher dynamic viscosity, and a lower sonic velocity than were the lab data. It is not surprising that the parameters resulting from the lab and flight tests differ quantitatively.

From data previously presented, it may be prematurely concluded that the solution to the problem of pneumatic distortion is to eliminate the pressure tubing altogether. If this were done, frictional damping would be eliminated and the sensor time lag would be reduced to zero. However, this conclusion is only partly true. As the tubing length and the damping ratio approach zero, the magnitude ratio of the first resonant peak grows rapidly.[1] At the same time, as the tubing length diminishes, the natural frequency of vibration begins to grow asymptotically. This resonant condition at high frequencies will tend to amplify turbulent noise greatly within the boundary layer itself. The amplified noise will overwhelm any pressure changes which are occurring outside of the boundary layer if the resonance is strong enough.

[1] At a magnitude ratio of 0.5 the amplitude ratio of the first resonant peak is 1.0 dB. This corresponds to an amplification factor of approximately 1.12. On the other hand, at a damping ratio of 0.05 the amplitude ratio of the first resonant peak is 13.7 dB. This corresponds to an amplification factor of 10.0.

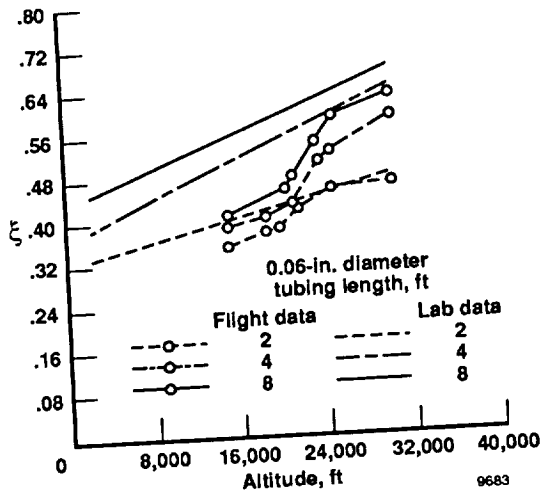

Figure 26. Lab and flight comparisons: damping ratio.

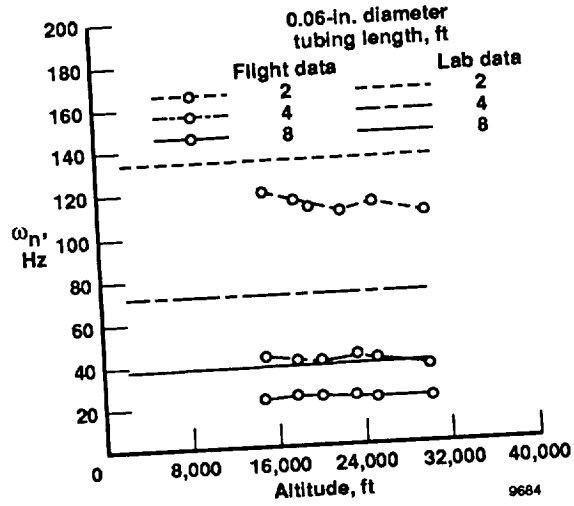

Figure 27. Lab and flight comparisons: natural frequency.

The system designer must take great care when attempting to obtain unsteady pressure measurements using pneumatic sensing systems. If a zero-volume configuration cannot be achieved, then the designer must be sure to provide pre-sample lowpass filtering with a rolloff frequency that is sufficiently lower than the expected resonance frequency of the sensing system.

CONCLUDING REMARKS

Laboratory and flight data were obtained which characterized the effects of pneumatic attenuation and resonance. Good qualitative agreement was demonstrated between the lab and flight data. Quantitative disagreements are probably caused by differing ambient temperatures for the lab and flight tests.

The data demonstrate that the behavior of conventional pneumatic pressure systems may be modeled as a second-order filter. The second-order filter model, as it is simple, may be used by the system designer to simulate the effects of pneumatic distortion of the pressure measurements. The model provided a convenient means of unifying and condensing the flight and laboratory data. Data, analyzed through the use of this model, show great consistency and predictability. The data as presented offer some insight into the appropriate structure of these model parameters.

More work still must be performed. The analogy of equation (1) and the complex wave equation of reference 2 should be carried further to provide a series of nondimensional parameters which hold over an entire range of altitudes and tubing geometries. These nondimensional parameters could be uniquely related to ξ and ω_n. Such a study may aid in reconciling some of the quantitative discrepancies between the lab and flight data.

Ames Research Center
Dryden Flight Research Facility
National Aeronautics and Space Administration
Edwards, California, October 10, 1989

APPENDIX

A considerable body of information is available concerning the effects of pneumatic distortion within remotely mounted pressure sensing devices. Early attempts to model the behavior of pneumatic distortion used the equations of momentum and continuity to predict the behavior of pressure sensing systems in terms of a first order lag (refs. 1 and 4). This approach, although simple and accurate for overdamped systems, does not allow for the resonant behavior which occurs in underdamped systems. This analysis is valid only for sensing systems in which large internal volumes are enclosed. References 2, 3, 5, and 6, have demonstrated that pressure variations at the surface propagate as longitudinal waves from the surface through the connective tubing to the transducer. The wave propagation is damped by frictional attenuation along the walls of the tubing. When the wave reaches the downstream end of the tubing, it is reflected back up the tube and may either damp or amplify incoming pressure waves. The combination of frictional damping and wave reflection manifests itself as a spectral distortion of the pressure response and produces both a magnitude change and a phase lag.

Reference 2 has demonstrated that this wave behavior may be described in terms of a single wave equation constrained by a set of bilinear boundary conditions. The model, verified by experimental results, predicts that multiple wave harmonics will occur for lightly damped sensing systems, and a nonresonant first-order type of response will occur for highly damped sensing systems. The model of reference 2 may be approximated by a second-order linear filter of the form

$$\frac{d\,P_M(t)^2}{d\,t^2} + 2\xi\omega_n \frac{d\,P_M(t)}{d\,t} + \omega_n^2 P_M(t) = \omega_n^2 P_I(t) \tag{1}$$

where $P_I(t)$ is the input pressure, and $P_M(t)$ is the measured pressure. The second-order model can be made to match the complicated wave behavior up to the second harmonic by properly selecting the damping ratio, ξ, and natural frequency, ω_n. For all but very large diameter or very short sections of pneumatic tubing, reference 6 has demonstrated that the magnitude of the second harmonic is far less than that of the first harmonic. Hence, the model of equation (1) is not greatly limited.

In this report, the parameters ξ and ω_n are to be determined from experimental results. The parameters are to be analyzed as a function of tubing geometry and pressure altitude to give a series of parametric curves. The parametric curves will be established based upon the results of both lab and flight experiments. Frequency response analysis techniques (ref. 7) will be used to identify the parameters.

For overdamped cases ($\xi \geq 1$), the damping ratio and natural frequency may be determined from the magnitude ratio, M_B, and frequency, ω_B, at which the magnitude rolls off asymptotically at 40 dB/decade. In this case

$$\omega_n = \omega_B$$

and

$$\xi = \frac{M_B}{2}$$

For underdamped sensing systems ($\xi < 1$), the damping ratio and natural frequency may be determined from the magnitude ratio, M_r, and frequency, ω_r, of the first resonant peak. In this case

$$\xi^4 - \xi^2 + \frac{1}{4\,M_r^2} = 0 \tag{2}$$

and

$$\omega_n = \frac{\omega_r}{\sqrt{1 - 2\xi^2}} \tag{3}$$

To relate the damping ratio and natural frequency of the system to a time lag, take the ratio of the phase angle divided by the natural frequency in the limit that the natural frequency approaches zero. The result is

$$\tau_L = -\frac{2\xi}{\omega_n}$$

Since τ_L is a redundant parameter, its values will not be explicitly given in this report.

REFERENCES

1. Irwin, K., *Lag in Aircraft Altitude Measuring Systems*, Defense Documentation Center for Scientific and Technical Information, Document AD 427017, Alexandria, VA, 1964.

2. Whitmore, S.A., *Formulation of a General Technique for Predicting Pneumatic Attenuation Errors in Airborne Pressure Sensing Devices*, NASA TM-100430, 1988.

3. Schuder, C.B., and R.C. Binder, "The Response of Pneumatic Transmission Lines to Step Inputs," *J. of Basic Engineering*, ASME Transactions, Dec. 1959.

4. Lamb, J.P., Jr., *The Influence of Geometry Parameters Upon Lag Error in Airborne Pressure Measurement Systems*, WADC TR 57-351, Wright-Patterson AFB, Ohio, July 1957.

5. Iberall, A.S., *Attenuation of Oscillatory Pressures in Instrument Lines*, National Bureau of Standards Research Paper, RP2115, July 1950.

6. Bergh, H., and H. Tijdeman, *The Influence of the Main Flow on the Transfer Function of Tube-Transducer Systems Used for Unsteady Pressure Measurements*, National Aerospace Laboratory report MP72023U, 1972. (Primary source—Bergh, H., and H. Tijdeman, *Theoretical and Experimental Results for the Dynamic Response of Pressure Measuring Systems*, NLR report F.238, 1965).

7. D'Azzo, J.J., and C.H. Houpis, *Feedback Control System Analysis and Synthesis, 2nd Edition*, McGraw-Hill Book Company, New York, 1966.

8. Stephens, R.W.B., and A.E. Bate, *Acoustics and Vibrational Physics*, St. Martin's Press, New York, 1966.

9. Schlichting, H., *Boundary Layer Theory*, McGraw-Hill Book Company, New York, 1960.

NASA National Aeronautics and Space Administration

Report Documentation Page

1. Report No.	2. Government Accession No.	3. Recipient's Catalog No.
NASA TM-4171		

4. Title and Subtitle

Experimental Characterization of the Effects of Pneumatic Tubing on Unsteady Pressure Measurements

5. Report Date

March 1990

6. Performing Organization Code

7. Author(s)

Stephen A. Whitmore, William T. Lindsey, Robert E. Curry, and Glenn B. Gilyard

8. Performing Organization Report No.

H-1538

10. Work Unit No.

RTOP 505-60-21

9. Performing Organization Name and Address

NASA Ames Research Center
Dryden Flight Research Facility
P.O. Box 273, Edwards, California 93523-5000

11. Contract or Grant No.

13. Type of Report and Period Covered

Technical Memorandum

12. Sponsoring Agency Name and Address

National Aeronautics and Space Administration
Washington, DC 20546

14. Sponsoring Agency Code

15. Supplementary Notes

Stephen A. Whitmore, Robert E. Curry, and Glenn B. Gilyard: Ames Research Center, Dryden Flight Research Facility, Edwards, California.
William T. Lindsey: Air Force Wright Aeronautical Laboratory, Wright-Patterson Air Force Base, Ohio.

16. Abstract

Advances in aircraft control system designs have, with increasing frequency, required that airdata be used as flight control feedback. This condition requires that these data be measured with accuracy and high fidelity. Most airdata information is provided by pneumatic pressure measuring sensors. Typically unsteady pressure data provided by pneumatic sensing systems are distorted at high frequencies. The distortion is a result of the pressure being transmitted to the pressure sensor through a length of connective tubing. The pressure is distorted by frictional damping and wave reflection. As a result, airdata provided all-flush, pneumatically sensed airdata systems may not meet the frequency response requirements necessary for flight control augmentation. Both laboratory and flight tests were performed at NASA Ames Research Center's Dryden Flight Research Facility to investigate the effects of this high-frequency distortion in remotely located pressure measurement systems. Good qualitative agreement between the laboratory and flight data are demonstrated. Results from these tests are used to describe the effects of pneumatic distortion in terms of a simple parametric model.

17. Key Words (Suggested by Author(s))

Airdata
Pneumatic lag
Pneumatic tubing
Pressure sensors

18. Distribution Statement

Unclassified — Unlimited

Subject category 06

19. Security Classif. (of this report)	20. Security Classif. (of this page)	21. No. of pages	22. Price
Unclassified	Unclassified	30	A03

For sale by the National Technical Information Service, Springfield, VA 22161-2171.

NASA FORM 1626 OCT 86

NASA-Langley, 1990